Correspondence - Characterization of the effective performance of a high-frequency annular-array-based imaging system using anechoic-pipe phantoms

NIH Public Access
Author Manuscript
IEEE Trans Ultrason Ferroelectr Freq Control. Author manuscript; available in PMC 2013 June 01.

Published in final edited form as:
IEEE Trans Ultrason Ferroelectr Freq Control. 2012 December ; 59(12): 2825–2830. doi:10.1109/TUFFC.2012.2525.

Characterization of the effective performance of a high-frequency annular-array based imaging system using anechoic-pipe phantoms

Erwan Filoux [Member, IEEE],
Riverside Research, F.L. Lizzi Center for Biomedical Engineering, New York, NY, USA

Jonathan Mamou [Senior Member, IEEE],
Riverside Research, F.L. Lizzi Center for Biomedical Engineering, New York, NY, USA

Carmel M. Moran,
Center for Cardiovascular Science, Queen's Medical Research Institute, University of Edinburgh, Edinburgh, UK

Stephen D. Pye, and
NHS Lothian, Royal Infirmary of Edinburgh, Edinburgh, UK

Jeffrey A. Ketterling [Senior Member, IEEE]
Riverside Research, F.L. Lizzi Center for Biomedical Engineering, New York, NY, USA

Erwan Filoux: efiloux@riversideresearch.org

Abstract

A resolution integral (RI) method based on anechoic-pipe, tissue-mimicking phantoms was used to compare the detection capabilities of high-frequency imaging systems based on a single-element transducer, a state-of-the-art, 256-element linear array or a 5-element annular array. All transducers had a central frequency of 40 MHz with similar conventionally measured axial and lateral resolutions (about 50 and 85 μm, respectively). Using the RI metric, the annular array achieved the highest performance ($RI = 60$), followed by the linear array (47) and the single-element transducer (24). Results showed that the RI metric could be used to efficiently quantify the effective transducer performance and compare the image quality of different systems.

I. Introduction

High-frequency (HF, >20 MHz) ultrasound imaging scanners are widely available and offer a broad range of features that can accommodate a variety of applications. HF systems are typically applied to ophthalmic [1], dermatological [2], small-animal [3] and intravascular imaging [4] applications. Parameters such as spatial resolution, transducer frequency, temporal resolution, signal-to-noise ratio (SNR) or contrast-to-noise ratio (CNR) must be considered when assessing the performance of a scanner and its suitability to a given application. The performance of a scanner is usually described in terms of depth-of-field (DOF) and spatial resolution at the geometric focus. Spatial resolution is usually measured with fiber-based phantoms [5], but these simple measurements do not take into account acoustic scattering and attenuation in real tissues. Tissue-mimicking (TM) phantoms can be used to provide a more realistic medium for device characterization because they simulate conditions more relevant to scanning within tissue. In a previous study [6], we characterized the detection capabilities of a custom HF imaging system based on an annular-array transducer, and two HF commercial scanners from VisualSonics (VisualSonics Inc., Toronto, ON, Canada): the Vevo 770 (single-element transducer) and Vevo 2100 (linear-array transducer). The characterization method was based on a TM phantom containing

anechoic spheres with sizes ranging from 1090 to 100 μm. The ability of the scanners to detect those spheres was dependent on their spatial resolution in all directions simultaneously (3D resolution). The CNR of the spheres was measured and used as a metric to compare the 3D resolutions and detection ranges of the scanners.

Here, we use an alternate approach to compare the detection capabilities of these ultrasound scanners. The approach was developed by Moran *et al.* to quantify the imaging performance of several commercial scanners for preclinical applications [7]. The method was based on images of anechoic pipes with diameters ranging from 7.9 to 0.045 mm that were embedded in a TM material. The depth range over which each pipe could be detected was plotted as a function of the pipe diameter, and the curve was integrated to calculate the resolution integral (RI). The RI metric system provided a single figure-of-merit that could be used to compare the performance of a wide variety of scanners that operated in the frequency range between 5 and 60 MHz [8].

All the transducers compared in this study had a central frequency of around 40 MHz and similar axial and lateral resolutions at the focus as measured using conventional methods. These characteristics are not sufficient to compare the performance of the scanners because their detection capabilities vary with depth and depend on the shape of the beam in all three dimensions. The RI approach was used to quantify the imaging performance of the different systems by determining effective values for their spatial resolution and DOF.

II. Materials and Methods

A. Anechoic pipe phantoms

The pipe phantoms used in this study were fabricated by Moran *et al.* [7], [9] and were composed of a series of wall-less anechoic pipes embedded in an agar-based TM background material with an attenuation coefficient of 0.5 dB/cm/MHz and speed of sound of 1540 m/s. The pipes were formed in several cylindrical blocks of the TM material, 60 mm in diameter and 40 mm in height, using wires of various diameters positioned at an angle of 40° to the vertical. Once the TM material had solidified, the blocks were immersed in a solution of water and glycerol, the wires were removed and the solution filled the wall-less pipes. The diameters of the pipes used in this study were 1470, 550, 330, 193, 139 and 92 μm.

B. Annular-array system

A 40 MHz annular-array transducer (Table I) was fabricated through a similar process as that described by Ketterling *et al.* [10]. The array was composed of five, equal-area rings of copolymer P(VDF-TrFE) with a total aperture of 6 mm and a geometric focus of 12 mm. A synthetic-focusing (SF) algorithm [11] was used in post-processing to focus the data acquired from the 25 transmit-to-receive combinations and create a composite image with multiple focal zones. With this beamforming approach, the DOF and the lateral resolution were optimized at all depths of the image.

The transducer was excited using a five-channel pulser/receiver from Daxsonics (Daxsonics Ultrasound Inc., Halifax, NS, Canada). The prototype pulser could independently send a very short impulse signal to any of the five elements, with a peak-to-peak voltage of 200 V and an amplification of 45 dB in receive. The RF data were acquired from all five channels simultaneously using 3 digitizer cards (PXI-5152, National Instrument, Austin, TX, USA) with 8-bit resolution and 250 MHz sampling rate. A motorized stage (LAL35, SMAC, Carlsbad, CA, USA) with 1-μm precision, driven by a motion-control card (PXI-7534, National Instruments), was used to mechanically scan the transducer across the pipe phantoms. Mechanical scanning, data acquisition and processing were performed using a

custom LabVIEW (National Intruments) program and up to 6 frames per second could be obtained for real-time imaging (useful when aligning the pipes with the plane of the scan).

Prior to imaging, the tip of the transducer was immersed in a mixture of water and glycerol and was positioned approximately 6 mm above the front surface of the phantom, so that the distance from the surface of the phantom to the focus of the transducer was comparable to that of the commercial systems (≈ 6 mm, see Table I). This ensured that the attenuation of the acoustic signals was similar for all systems.

C. Commercial systems

Two state-of-the-art, high-resolution scanners were used to image the phantoms. For each system, a 40 MHz probe with 6 mm focal distance was used and spatial resolutions at the focus were close to that of the annular array (Table I). The Vevo 770 probe (RMV-704) was composed of a single-element transducer with a 3 mm aperture, and mechanically scanned in a sectorial motion to make a B-mode image. The RF signals were acquired using an external digitizer card (Acqiris DP310, Agilent Technologies Inc., Santa Clara, CA) at 12-bit resolution and a 250 MHz sampling rate. To form the final image required to calculate the RI, envelope detection and log compression were performed using custom MATLAB (The MathWorks, Natick, MA, USA) software. The Vevo 2100 probe (MS-550D) was a linear-array transducer of 256 elements with a 6 mm radius of curvature in the elevation direction and up to three dynamic focal zones in the azimuth direction could be selected by the user. B-mode images were exported in TIF format and directly used to calculate the RI of the system.

With both systems, the probes were clamped perpendicular to the surface of the phantom and immersed in water and glycerol. The tip of the probes was softly pressed on the surface of the phantom so that the focus was located around 6 mm inside the TM material.

D. Data acquisition

Each system was used in a real-time imaging mode to properly position the probe such that the anechoic pipes were scanned along their longitudinal axis. In the case of the single-element transducer, the focus was fixed and a single image was sufficient to determine the range over which each pipe could be detected. With the other systems, optimal visualization of the proximal and distal parts of each pipe required the acquisition of two separate images. With the annular array, each pipe could not be completely visualized within the field-of-view of the system so the transducer had to be repositioned. When using the linear array, the whole pipe could be visualized in the same image but a maximum of three simultaneous focal zones, 1 or 2 mm apart, could be set at various depths in the image. The focal zones were first set to visualize the proximal part of each pipe and then the distal one. The imaging parameters of all three systems were set by a trained observer to optimize the visualization of the pipes and to ensure that the best image quality was provided under regular operation of the scanners.

E. Resolution Integral, characteristic resolution and DOF

The acquired B-mode images were used to calculate the RI, which represented the ratio of the effective detection range over the effective beamwidth of the scanner [12]. A scanner with large detection range and small beamwidth will have a high RI. Therefore, RI can be used to quantify and compare the performance of different imaging systems and transducers.

A visual assessment of the minimum and maximum depths at which the pipes were clearly resolved was performed using the acquired images. The assessment method was described in previous studies [8], [12] where it was carried out by trained observers to measure the

detection range of various scanners. In this study, the depth range L over which the pipes could be visualized was determined by the same observers so as to ensure consistency of the results. The values of L were plotted against the reciprocal of the corresponding effective pipe diameters $a = 1/D$. The effective pipe diameter $D=d/\sqrt{\cos(40°)}$ was calculated as the geometric mean of the pipe diameter in the image and elevation planes where d was the true pipe diameter. RI was defined as the value of the area under the curve $L(a)$ [12],

$$RI=\int_0^\infty L(\alpha)\,\mathrm{d}\alpha. \quad (1)$$

The intersection of the $L(a)$ curve (Fig. 1) with the ordinate (L_0) was defined as the maximum depth in the phantom at which signals from the speckle background could be visualized against the noise. This can be interpreted as the value of L that would be measured when scanning a pipe of infinite diameter ($a = 0$) and it was called the low contrast penetration (LCP) [12]. The intersection of $L(a)$ with the abscissa was defined by the reciprocal of the effective diameter of the smallest pipe that could be detected with the transducer (D_0).

The $L(a)$ curve was used to calculate L_R and D_R such as defined in Fig. 1 with $RI = L_R/D_R$. To maintain consistency with previous publications, L_R will be called the DOF and D_R the characteristic resolution of the scanner. These parameters, not to be confused with those reported in Table I, provided an estimate of the effective spatial resolution (in the azimuth and elevation directions simultaneously) of a transducer over its effective detection range and represent an ideal transducer with a collimated beam having a constant characteristic resolution D_R over a DOF L_R.

III. Results and Discussions

A. Detection performances

Figure 2 shows images of the phantoms acquired with each scanner along the longitudinal section of the anechoic pipes. The minimum (proximal) and maximum (distal) depths at which the pipes could be detected are shown. With the commercial single-element transducer [Fig. 2(a)] both the proximal and distal portions of the pipes could be visualized in a single image. The largest pipe (Fig. 2(a1)) could be resolved over a large depth range (almost 7 mm) despite the narrow DOF of the transducer (as reported in Table I). The proximal section of the pipe could be observed around 2 mm from the transducer with an apparent diameter quickly decreasing due to the fast drop in spatial resolution of the single-element transducer outside the focal zone (≈5–7 mm). The distal section of the pipe was observed around 9 mm because the SNR was too low to detect anything farther from the transducer. As the diameter of the pipes decreased [Fig. 2(a2)–(a5)], so did the range of detection but even the smallest visible pipe [Fig. 2(a5)] could still be clearly resolved around the focus of the transducer.

With the other scanners [Fig. 2(b)–(c)] multiple focal zones could be used (prior to or after data acquisition) to optimize the visualization of each part of the pipe. The commercial linear array allowed for three simultaneous focal zones to be defined. The best overall image quality would be obtained by placing the focal zones at 4, 6 and 8 mm (around the geometric focus), but it would not provide the best possible visualization of the proximal and distal parts of the pipes. By situating the focal zones at 2, 4 and 6 mm, the proximal part of the largest pipe [Fig. 2(b1), left image] could be resolved as close as 1 mm from the transducer, *i.e.*, at the surface of the phantom. To image the distal part of the pipe, the focal zones were shifted to 10, 12 and 14 mm [Fig. 2(b1), right image]. The pipe could be detected as far as 15 mm from the transducer, which is the limit of the field of view of the scanner (potentially

the largest pipe could be visualized deeper in the phantom). Compared to the single-element transducer [Fig. 2(a1)], the improved resolution of the linear array outside its geometric focus resulted in increased detection range and the apparent diameter of the pipe remaining fairly constant at all depths [Fig. 2(b1)]. The detection range L decreased rapidly with the diameter of the pipe [Fig. 2(b2)–(b5)] and it was almost as low as that of the single-element transducer for the 193 μm pipe [Fig. 2(b4)]. The 139 μm pipe could not be clearly resolved and was barely detected around the geometric focus of the transducer [Fig. 2(b5)]. This confirmed that the spatial resolution of the linear array was lower than that of the single-element transducer at the geometric focus, as expected from Table I.

In the case of the annular-array transducer [Fig. 2(c)] the larger pipe could also be resolved over a large depth range, from the surface of the phantom at 6 mm to around 17 mm away from the transducer. Compared to the linear array, the contrast of the pipes and the LCP were lower, resulting in a narrower detection range for the larger pipes [Fig. 2(c1)–(c3)]. But the decrease in detection range was not as steep as with the linear array, especially for the smallest pipes of 193 and 139 μm. When using the linear array to image the 330 and 193 μm pipes [Fig. 2(b3)–(b4)], the detection range L decreased steeply from around 9 mm for the 330 μm pipe to only 3.5 mm for the 193 μm one. Using the annular array, the detection range remained almost the same, with 8.1 mm for the 330 μm pipe [Fig. 2(c3)] and 6.8 mm for the 193 μm one [Fig. 2(c4)]. The annular array was also able to clearly resolve the 139 μm pipe over 6.2 mm [Fig. 2(c5)]. This showed that despite the better contrast and SNR provided by the linear array, the annular array had a higher effective resolution and enabled a better detection of the pipes smaller than 200 μm. A similar result was found in a previous study [6] using phantoms with anechoic spheres 200 μm in diameter.

B. Resolution Integral

The images in Fig. 2 were used by the trained observers to measure the depth range L over which each pipe could be resolved and the $L(\alpha)$ curves of each system are plotted in Fig. 3. None of the systems were able to resolve the 92 μm pipe so the corresponding value of L at $\alpha = 9.5\ \text{mm}^{-1}$ was 0 for all three systems. The imaging performances of the systems, described in Section III. A in terms of effective detection range and spatial resolution, can be deduced from the shape of the curves. For instance, it is easy to see that the effective resolution of the annular array (*i.e.*, the width of the acoustic beam) is below 193 μm ($\alpha \approx 4.5\ \text{mm}^{-1}$) over a depth range almost twice as large as that of the linear array. A more precise description of the evolution of the beam width as a function of depth could be deduced by obtaining $L(\alpha)$ curves from pipes with diameters more closely spaced. Comparing the shape of the curves of Fig. 3 with Fig. 1, the annular-array system is closest in shape to the curve for a transducer with a collimated beam.

The areas under the curves in Fig. 3 were calculated and the values of RI are summarized in Table II. The value of RI for the single-element transducer was almost half that of the linear array. From this single value one can deduce that the overall image quality of the Vevo 770 was lower than that of the Vevo 2100 system. An even higher RI value was obtained with the annular array as it could detect smaller pipes over a greater range of depths. The DOF and characteristic resolution were calculated to more precisely quantify the imaging performances of the different systems (Table II). The calculated characteristic resolution of the annular array (≈130 μm) was significantly better than that of the linear array (≈250 μm) but its DOF was around 3 mm narrower.

These effective values are in good agreement with the observations in Section III. A and are also consistent with the previous values of RI reported by Moran *et al.* [7], [8] for the single-element probe (RMV-704, $RI = 25$) and the linear-array probe (MS-550D, $RI = 47$). The commercial linear-array-based system obtained the best score when compared to many other

commercial scanners, which means that the imaging performances of the annular-array-based system can accommodate the most demanding HF applications requiring high-quality images. The superior resolution of the annular array (and single-element transducer) partly come from the radial symmetry of the beam. The synthetic-focusing algorithm used with the custom system maintains this optimal resolution across the DOF of the transducer, compared to the linear array whose resolution in the elevation direction is only optimal at the geometric focus. This study showed that, despite similar beam characteristics as measured using conventional techniques, the annular-array system provided higher effective performances than the other scanners because it combines fine resolution and wide DOF. This ability of the RI method to quantify effective detection capabilities makes it a useful tool for assessing the suitability of a scanner to a particular study. For applications such as imaging the anterior segment of the eye [1] or the brain ventricles of mouse embryos [13] where small features (≈200 μm) must be resolved over large depths (≈ 10 mm), the RI method showed that the annular-array system would provide the best performances.

IV. Conclusion

The imaging performances of three ultrasound scanners using a single-element, linear-array or annular-array transducer were characterized and compared using the RI method. Anechoic-pipe phantoms were used to measure the range over which anechoic pipes of various diameters, embedded in a TM material, could be visualized. The RI was calculated from these measurements and was used to quantify the imaging capabilities of the different systems, as well as their effective depth-of-field and spatial resolution. The RIs of the linear and annular arrays were twice as large as that of the single-element transducer, which was consistent with the significantly higher quality of the images displayed by these scanners. The single-element transducer provided a high effective resolution but the smallest effective DOF. The linear array showed the largest effective DOF but the lowest effective resolution. The custom system based on an annular array achieved the best imaging trade-off with both a high resolution and a wide DOF.

These results demonstrate that the RI approach allows for an efficient comparison of the performance of different systems, and it can be used as a single figure-of-merit metric for the assessment of equipment aging. One limitation of this method is that it is based on a specific phantom. In future work, it would be interesting to use phantoms with different shapes and material properties to better mimic particular tissues and imaging conditions.

Acknowledgments

This research was supported by the National Institutes of Health (EB008606). C.M. Moran would like to acknowledge funding from The Wellcome Trust (WT083227AIA). The authors thank O. Aristizábal for his help with the acquisition of data from the commercial scanners.

References

1. Silverman RH, Ketterling JA, Coleman DJ. High-frequency ultrasonic imaging of the anterior segment using an annular array transducer. Ophthalmology. 2007; 114(4):816–822. [PubMed: 17141314]
2. Turnbull DH, Starkoski BG, Harasiewicz KA, Semple JL, From L, Gupta AK, Sauder DN, Foster FS. 40–100 MHz B-scan ultrasound backscatter microscope for skin imaging. Ultrasound in Med & Biol. 1995; 21(1):79–88. [PubMed: 7754581]
3. Foster FS, Pavlin CJ, Harasiewicz KA, Christopher DA, Turnbull DH. Advances in ultrasound biomicroscopy. Ultrasound in Med & Biol. 2000; 26(1):1–27. [PubMed: 10687788]
4. de Korte CL, Van der Steen AFW, Céspedes EI, Pasterkamp G, Carlier SG, Mastik F, Schoneveld AH, Serruys PW, Bom N. Characterization of plaque components and vulnerability with

intravascular ultrasound elastography. Phys Med Biol. 2000; 45(6):1465–1475. [PubMed: 10870704]

5. Goodsitt MM, Witt S, Hykes DL, Kofler JM. Real-time B-mode ultrasound quality control test procedures. Report of AAPM ultrasound task group no. 1. Med Phys. 1998; 25(8):1385–1406. [PubMed: 9725125]
6. Filoux E, Mamou J, Aristizábal O, Ketterling JA. Characterization of the spatial resolution of different high-frequency imaging systems using a novel anechoic-sphere phantom. IEEE Trans Ultras Freq Cont. 2011; 58(5):994–1005.
7. Moran CM, Ellis W, Pye SD, Smart S. Characterising the performance of a high resolution ultrasound scanner for pre-clinical ultrasound imaging. IEEE Ultras Symp. 2008:1724–1727.
8. Moran CM, Pye SD, Ellis W, Janeczko A, Morris KD, McNeilly AS, Fraser HM. A comparison of the imaging performance of high resolution ultrasound scanners for preclinical imaging. Ultrasound in Med & Biol. 2011; 37(3):493–501. [PubMed: 21256667]
9. Pye, SD.; Ellis, W. Assessment of image quality. British Patent Application. 0228768.8. 2002.
10. Ketterling JA, Aristizábal O, Turnbull DH, Lizzi FL. Design and fabrication of a 40-MHz annular array transducer. IEEE Trans Ultras Freq Cont. 2005; 52(4):672–681.
11. Ketterling JA, Ramachandran S, Aristizábal O. Operational verification of a 40-MHz annular array transducer. IEEE Trans Ultras Freq Cont. 2006; 53(3):623–630.
12. MacGillivray TJ, Ellis W, Pye SD. The Resolution Integral: visual and computational approaches to characterising ultrasound images. Phys Med Biol. 2010; 55(17):5067–5088. [PubMed: 20702928]
13. Aristizábal O, Ketterling JA, Turnbull DH. 40-MHz annular array imaging of mouse embryos. Ultrasound in Med & Biol. 2006; 32(11):1631–1637. [PubMed: 17112949]

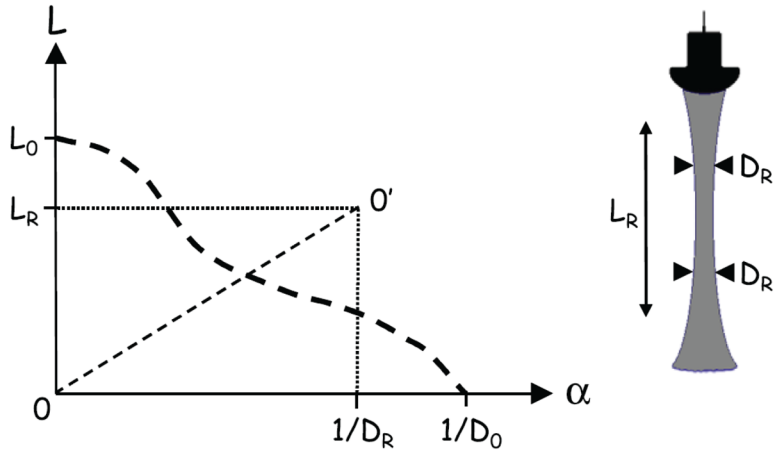

Fig. 1.

Example of a $L(\alpha)$ curve (dashed line) for an ultrasound beam with low-contrast penetration L_0, minimum resolution D_0, DOF L_R and characteristic resolution D_R. RI is equal to the area under $L(\alpha)$. Line $00'$ bisects this area and point $0'$ is defined such that $RI = L_R/D_R$.

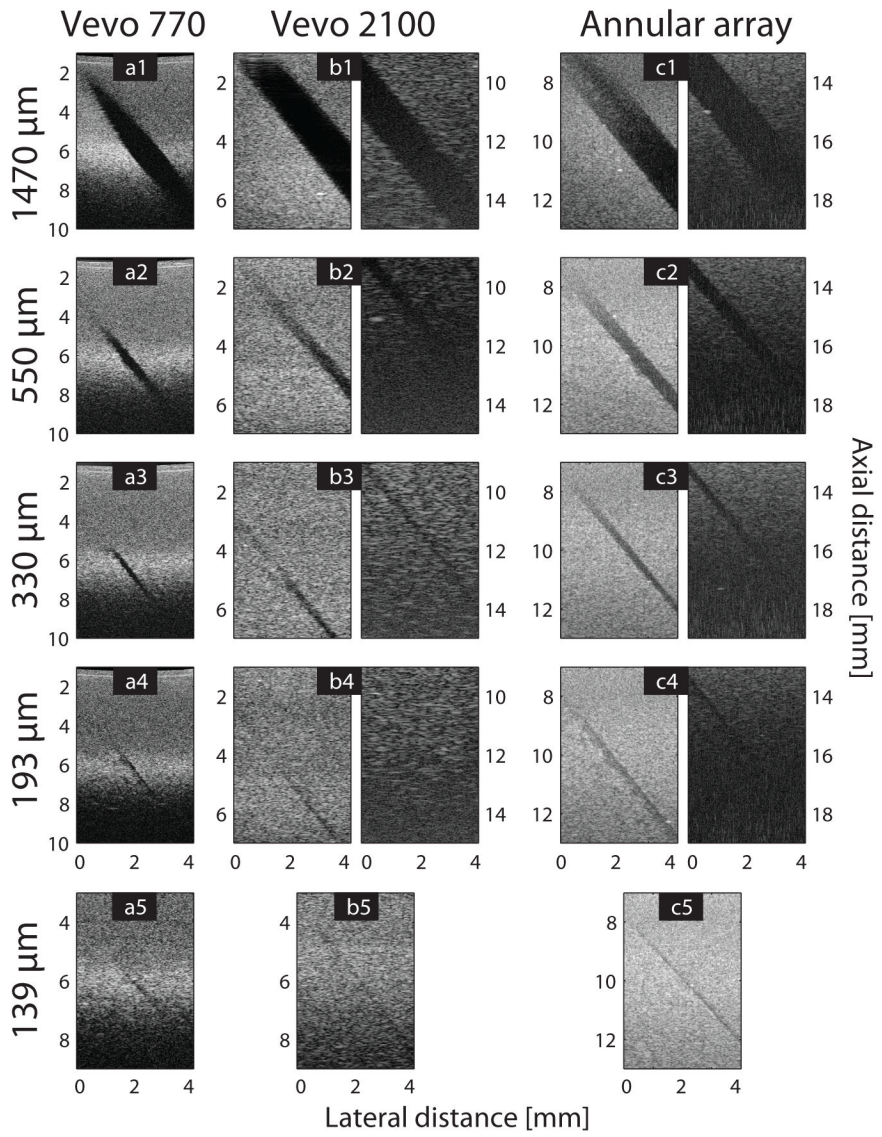

Fig. 2.

Images of the anechoic pipes of diameter 1) 1470, 2) 550, 3) 330, 4) 193 and 5) 139 μm acquired with the a) Vevo 770, b) Vevo 2100, and c) custom system. In cases where two images were used to visualize the proximal (left image) and distal (right image) parts of a pipe, the axial distance (*i.e.*, the distance from the transducer) was displayed on the left or right side of the corresponding image. For each image the focal zone and position of the transducer were set to optimize the visualization of the pipe in the region of interest. A single image was used when the focal zone could not be varied (a) or when the pipe was barely resolved (b5 and c5). The images are displayed with a dynamic range of 35 dB for the Vevo 770 scanner (a) and 65 dB for the other systems (b and c).

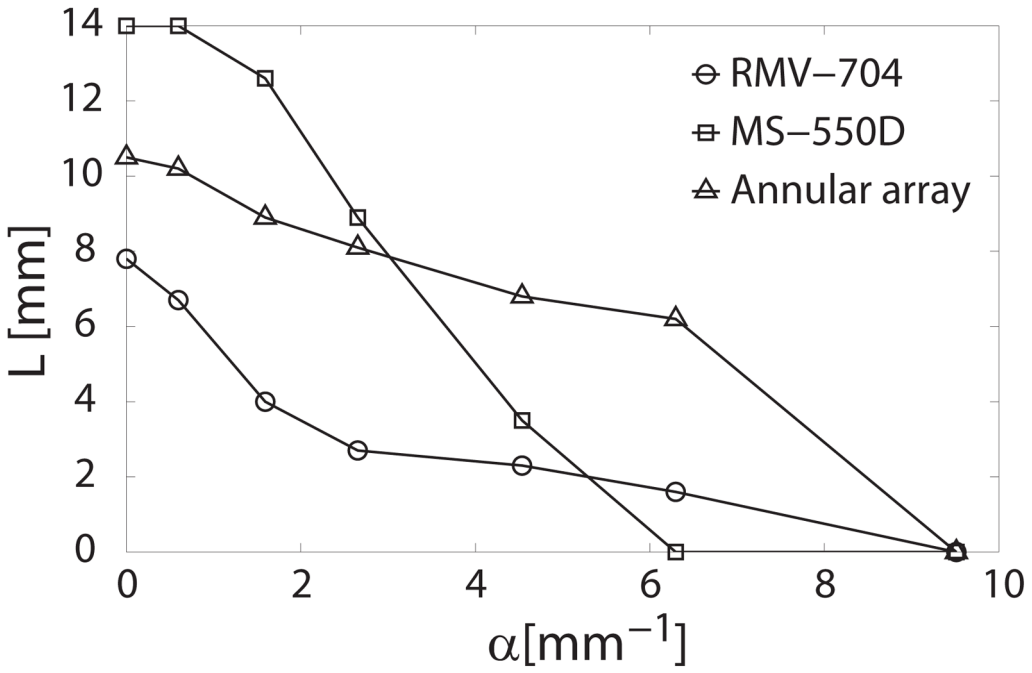

Fig. 3.
Plot of the detection range L of the anechoic pipes as a function of the reciprocal effective pipe diameter, a, for the single-element transducer (RMV-704), linear array (MS-550D), and annular array.

TABLE I

Transducer characteristics

Scanner	Probe	Transducer type	f_c (MHz)	R_{ax} (μm)	R_{lat} (μm)	F (mm)	DOF (mm)	D_{ph} (mm)
Vevo 770	RMV-704	Single-element	40	40	80	6	1.5	1
Vevo 2100	MS-550D	Linear-array	40	40	90	6	-	1
Custom	-	Annular-array	40	60	85	12	6	6

f_c = central frequency; R_{ax} = axial resolution; R_{lat} = lateral resolution at the focus; F = geometric focal distance; DOF = depth-of-field; D_{ph} = distance between the transducer and the surface of the phantom.

TABLE II

Scanners performances[1]

Scanner	*RI*	L_R (mm)	D_R (μm)
Vevo 770	24	3.8	158
Vevo 2100	47	11.5	247
Annular array	60	7.9	128

[1] RI = resolution integral; L_R = DOF; D_R = characteristic resolution.